ACS OMEGA

http://pubs.acs.org/journal/acsodf

Article

Effect of Different Modification Methods on the Adsorption of Manganese by Biochar from Rice Straw, Coconut Shell, and Bamboo

Guoliang Chen,* Khamphouvanh Viengvilay, Weijian Yu, Teng Mao, Zhihui Qu, Bixin Liang, Zhang Chen, and Zhixian Li

Cite This: *ACS Omega* 2023, 8, 28467−28474

Read Online

ACCESS | Metrics & More | Article Recommendations

ABSTRACT: The adsorption capacity of pristine biochar without modification is usually low. In this experiment, we comprehensively evaluated the adsorption of Mn(II) by biochar with different modification methods from different biomass. The biochar from rice straw, coconut shell, and bamboo was produced by pyrolysis at 600 °C under nitrogen and then modified with HNO_3, NaOH, and Na_2S, respectively. The results showed that the adsorption capacities of these modified biochar samples were in the order Biochar-NaOH > Biochar-Na_2S > Biochar-HNO_3. Among the three modification methods, biochar modified with NaOH is the optimum for the adsorption of Mn(II). However, the same method of modification has different effects on different biomass feedstocks. Rice straw: R-C > R-NaOH-C > R-Na_2S-C > R-HNO_3-C; coconut shell: C-NaOH-C > C-Na_2S-C > C-HNO_3-C > C-C; bamboo: B-NaOH-C > B-Na_2S-C > B-C > B-HNO_3-C. At the pH of 5 and 30 °C, R-C, C-NaOH-C, and B-NaOH-C showed the highest maximum adsorption capacity for Mn(II). Equilibrium data were evaluated by Langmuir, Freundlich, and Temkin isotherm models, and the results suggested that the Langmuir model is the most suitable to expound the adsorption behavior of Mn(II) on R-C, C-NaOH-C, and B-NaOH-C. Overall, the results from this work suggest that the key for preparing biochar adsorbents with high capacity is to choose the appropriate biomass feedstock and modification method.

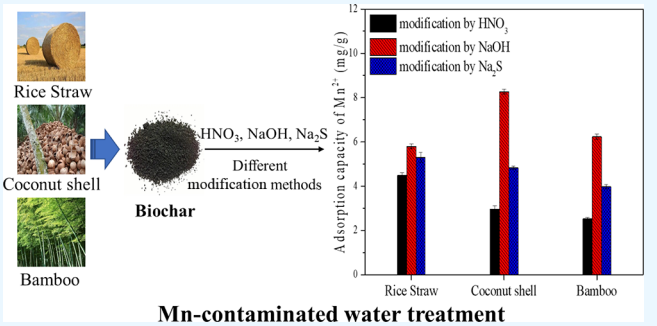

1. INTRODUCTION

Manganese (Mn) is an essential element for living organisms.[1] However, excess manganese in the environment is very harmful. It can cause humans headache and memory loss and stress on the growth of plants.[2,3] The World Health Organization suggested that the Mn concentration in drinking water should be less than 0.05 mg/L. With the rapid development of the manganese mining and industry, the concentration of Mn in water is increasing. It has preoccupied a growing number of scientists in recent years.[4]

Biochar has been widely used as adsorbents for removing pollutants from water and wastewater due to its special surface structure.[5] Numerous factors including feedstocks and operation parameters of the pyrolysis process (temperature, duration, heating rate, and pressure) affect the yield and quality of biochar. However, the adsorption capacity of pristine biochar without modification is usually very low.[6,7] Modification typically changes the properties of biochar and increases the adsorption capacity to numerous pollutants. Functional groups on biochar surfaces can be classified into several groups: O-containing groups (e.g., carboxylic groups, phenolic groups, and lactonic groups), N-containing groups (e.g., amine-N groups, pyrrolic-N groups, and graphitic-N groups), S-containing groups (e.g., sulfonic groups), and other functional groups.[5,8] The results of previous studies indicated that the feedstock or biochar modified by acids, bases, or metal salts can enhance the adsorption capacity of pristine biochar by introducing additional functional groups onto their surfaces.[9−11]

Therefore, this study was to comprehensively evaluate the mechanism of chemical modification methods (HNO_3, NaOH, and Na_2S) on enhancement of the adsorption capacity of biochar adsorbents for Mn(II) removal and find out the promising modification method. This experiment was based on low-cost, wide-ranging rice straw, coconut shell, and bamboo feedstock. This work will provide support for the preparation of biochar with high adsorption capacity and solving the problems caused by agricultural and forestry waste.

Received: April 21, 2023
Accepted: July 18, 2023
Published: July 26, 2023

2. MATERIALS AND METHODS

2.1. Preparation of Biochar and Modified Biochar. Rice straw, coconut shell, and bamboo branch feedstocks were collected from Xiangtan, Hunan Province, China. All the biomass feedstocks were washed with distilled deionized water several times and dried at 60 °C for 48 h. The dried biomass was filled into the crucible and compacted and placed in a box-type atmosphere furnace (JQF1100-3, Shanghai Jiugong Electric Co., Ltd., China) for pyrolysis at 600 °C under the protection of nitrogen for 2 h. The obtained biochar was ground into powder (<0.154 mm) and stored in a sealed bag before use.[12,13] The rice straw biochar was recorded as R-C, the coconut shell biochar was recorded as C-C, and the bamboo biochar was recorded as B-C.

To prepare modified biochar, 20 g of obtained biochar was placed in three 500 mL beakers, and 200 mL of 10% HNO_3, 3 mol/L NaOH, and 1.5 mol/L of Na_2S were added, respectively. The mixtures were stirred continuously with a speed of 150 rpm for 180 min at 25 °C and then separated by filtration. The samples were repeatedly washed with deionized water until the pH of the filtrate was nearly neutral and then were oven-dried again at 60 °C for 24 h. The nitric acid-modified rice straw biochar was recorded as R-HNO_3-C, the sodium hydroxide-modified rice straw biochar was recorded as R-NaOH-C, and the sodium sulfide-modified rice straw biochar was recorded as R-Na_2S-C. The nitric acid-modified coconut shell biochar was recorded as C-HNO_3-C, the sodium hydroxide-modified coconut shell biochar was recorded as C-NaOH-C, and the sodium sulfide-modified coconut shell biochar was recorded as C-Na_2S-C. The nitric acid-modified bamboo biochar was recorded as B-HNO_3-C, sodium hydroxide-modified bamboo biochar was recorded as B-NaOH-C, and sodium sulfide-modified bamboo biochar was recorded as B-Na_2S-C.

2.2. Properties of Biochar. *2.2.1. Biochar Yield.* The mass of the crucible was M_0; the crucible was filled and compacted with biomass, and the mass was M_1. It was subjected to pyrolysis in a box-type atmosphere furnace under a N_2 atmosphere, and the mass was M_2 after natural cooling. The biochar yield ($W_{biochar}$) was calculated following eq 1:

$$W_{biochar} = \frac{M_2 - M_0}{M_1 - M_0} \times 100\% \quad (1)$$

2.2.2. Biochar Ash and pH. The ash content of biochar was measured by referencing to "Experimental Methods for Charcoal and Charcoal" (GB/T177664-1999). We weighed about 400 ± 0.1 g of the biochar sample and recorded it as M_0. We placed it into the bottom of the crucible and then weighed the mass M_1. We opened and placed it in a high-temperature electric furnace, kept at 800 °C for 4 h, and naturally cooled it to give a mass M_2. The calculation formula for the ash content (W_{ash}) of biochar is shown in eq 2:

$$W_{ash} = \frac{M_2 - M_1 + M_0}{M_0} \times 100\% \quad (2)$$

The pH of biochar was measured with a pH meter according to the method of Chen et al.[14]

2.3. Batch Adsorption Experiments. *2.3.1. Adsorption of Pristine Biochar and Modified Biochar.* Fifty and 100 mg of pristine biochar and modified biochar were added to 50 mL of 10, 50, and 100 mg/L $MnCl_2$ solution with a pH of 5 (adjusted with 1 mol/L NaOH or HCl) in a 150 mL conical flask. The mixtures were shaken in a thermostatic shaker at 25 °C for 3 h and then filtered. The concentration of Mn^{2+} in the supernatant was measured by an atomic absorption spectrophotometer (Agilent 240FS, USA). The removal rate (E) and adsorption capacity (Q) were calculated by eqs 3 and 4:[5]

$$E = \frac{C_0 - C_t}{C_0} \quad (3)$$

$$Q = \frac{C_0 - C_t}{W} \times V \quad (4)$$

C_0 (mg/L) is the Mn^{2+} concentration in solution; C_t (mg/L) is the Mn^{2+} concentration in solution at time t; W (g) is the mass of the adsorbent; V (L) is the volume of solution; Q (mg/g) is the adsorption capacity. The biochar that had the maximal adsorption capacity was selected for the subsequent experiments.

2.3.2. Biochar Dosage, pH, and Temperature. To investigate the influence of the biochar dosage on the adsorption of Mn^{2+}, 10, 50, 100, 150, 200, 250, 300, 350, and 400 mg of biochar were added to 50 mL of 50 mg/L $MnCl_2$ solution, respectively. The influence of pH and temperature experiments were carried out by mixing 50 mg of biochar and 50 mL of $MnCl_2$ solution with a series of different pH (2, 3, 4, 5, 6, and 7, adjusted with 1 mol/L NaOH or HCl) and at different temperatures (20, 25, 30, 35, and 40 °C), respectively.

All the mixtures were shaken in a thermostatic shaker for 3 h to achieve equilibrium and then filtered. The concentration of Mn^{2+} in the supernatants was measured by an atomic absorption spectrophotometer.

2.3.3. Adsorption Kinetics and Isotherms. For adsorption kinetics, 50 mg of biochar and 50 mL of 50 mg/L $MnCl_2$ solution were added into a 250 mL conical flask. The pH of the mixture was adjusted to around 5, shaken at 25 °C, and sampled at 10, 20, 30, 60, 120, 180, 300, 480, 720, 1080, and 1680 min. The adsorption isotherm experiment was carried out by mixing 50 mg of biochar and 50 mL of different concentrations of $MnCl_2$ solution (10, 20, 30, 40, 50, 75, 100, 150, and 200 mg/L) at 25 °C for 3 h. All samples were measured immediately after separation.

2.3.4. Statistical Analysis. Each experimental treatment was conducted in triplicate to reproduce conditions, and the results were presented as the means of each treatment. Graphical work was carried out using Origin 8.0 (OriginLab Corporation, Northampton, MA, USA).

3. RESULTS AND DISCUSSION

3.1. Properties of Biochar. The yield, ash, and pH data of different biochar samples are displayed in Table 1.

As shown in Table 1, the biochar yields of rice straw, coconut shell, and bamboo are 33.86, 34.69, and 27.88%, respectively. The major nonash content of biomass feedstock is lost during pyrolysis. The adsorption capacity of biochar is usually related with the surface area, functional groups, and components of biochar.[15,16] Chemical modification has been reported to enhance its performance as an amendment or absorbent by introducing additional functional groups onto its surfaces.[17,18] After modification by HNO_3, NaOH, and Na_2S, there were significant differences among the pH and ash content of obtained biochar. It may be caused by the change of the surface area, functional groups, and components during the modification process, and the surface area, functional groups,

https://doi.org/10.1021/acsomega.3c02685
ACS Omega 2023, 8, 28467−28474

Table 1. Biochar Yield, Ash, and pH

biocharcoal	yield (%)	ash content (%)	pH value
R-C	33.86	32.78	10.12
R-HNO_3-C		25.43	3.24
R-NaOH-C		15.07	8.50
R-Na_2S-C		16.75	8.65
C-C	34.69	6.75	9.70
C-HNO_3-C		2.75	4.20
C-NaOH-C		3.42	8.43
C-Na_2S-C		3.95	8.92
B-C	27.88	7.93	9.49
B-HNO_3-C		4.32	3.14
B-NaOH-C		3.97	7.99
B-Na_2S-C		4.70	8.21

and components of obtained biochar are associated with modifying reagents. This was in agreement with other research results.[19−22]

3.2. Comparison of Different Modification Methods. In general, it is recognized that surface areas and functional groups of biochar increased during the chemical modification process, which is important for enhancing its contaminant sorption ability.[23,24] The results of adsorption experiments by R-C, R-HNO_3-C, R-NaOH-C, and R-Na_2S-C on different concentrations of manganese ion solution are displayed in Table 2.

As seen from Table 2, with the increase of Mn^{2+} in solution, the adsorption capacity of manganese ions by the unmodified biochar and modified biochar increased. The order of Mn^{2+} adsorption capacities by this biochar was as follows: rice straw, R-C > R-NaOH-C > R-Na_2S-C > R-HNO_3-C; coconut shell, C-NaOH-C > C-Na_2S-C > C-HNO_3-C > C-C; bamboo, B-NaOH-C > B-Na_2S-C > B-C > B-HNO_3-C. Among the three modification methods, biochar modified with NaOH was the optimum for manganese ion removal. It may be due to ash, condensed organic matter of biochar dissolved, and the surface basicity increase during modification with NaOH, which is beneficial for adsorption. For coconut shell and bamboo, C-NaOH-C and B-NaOH-C had the maximum adsorption capacity. However, for rice straw, the results of modification were not ideal. The adsorption capacities of R-NaOH-C, R-Na_2S-C, and R-HNO_3-C at different manganese ion concentrations were lower than that of R-C without modification. Modification with alkali led to the micropore volume of biochar to be decreased and thus resulted in a smaller surface.[25−27] This is disadvantageous for adsorption. The results indicated that the same method of modification had different effects on different biomass feedstocks. The physical and surface chemical properties of biochar or biomass feedstock should be carefully considered in the selection of pretreatment methods.

Therefore, the unmodified biochar R-C, B-NaOH-C, and C-NaOH-C were selected for the subsequent experiments.

3.3. Effect of the Adsorbent Dosage. It is very necessary to find the appropriate dosage of biochar for manganese ion removal. The results of R-C, C-NaOH-C, and B-NaOH-C are shown in Figure 1.

Figure 1 indicates that the removal rate of manganese ions increased with the increase of the biochar dosage. When the dosage of R-C was above 200 mg, C-NaOH-C was above 350 mg, and B-NaOH-C was above 400 mg, the adsorbent and adsorbate in the solution achieved equilibrium[26,28] and the removal rate no longer increased and approached fixed values: 97.2, 94.9, and 92.75%, respectively. A higher adsorbent dosage in the solution can provide more adsorptive sites.[29] However, the adsorption capacity of R-C, C-NaOH-C, and B-NaOH-C increased first and then decreased with the increase of the dosage. When the concentrations of biochar in the solution reached a certain value, the chance of biochar particles colliding with each other is greatly increased and formed agglomerated particles, which led to a decrease in the adsorption of Mn^{2+}. The maximum adsorption capacity of R-C, C-NaOH-C, and B-NaOH-C for manganese ions was 21.44, 9.51, and 7.04 mg/g, respectively.

Table 2. Adsorption Experiments of Unmodified and Modified Biochar[a]

			adsorption capacity of Mn^{2+} (mg/L)			
biomass	biochar dosage (mg)	Mn^{2+} concentration in solution (mg/L)	biochar	Biochar-HNO_3	Biochar-NaOH	Biochar-Na_2S
rice straw	50	10	10.00 ± 0.37	1.53 ± 0.04	2.36 ± 0.06	1.98 ± 0.04
		50	20.29 ± 0.50	4.49 ± 0.12	5.80 ± 0.10	5.30 ± 0.23
		100	22.82 ± 1.10	5.02 ± 0.04	6.43 ± 0.30	6.05 ± 0.11
	100	10	10.00 ± 0.26	1.97 ± 0.06	3.53 ± 0.12	2.77 ± 0.23
		50	22.04 ± 0.63	4.68 ± 0.17	8.17 ± 0.32	6.83 ± 0.16
		100	23.18 ± 0.83	5.60 ± 0.07	8.54 ± 0.25	7.39 ± 0.07
coconut shell	50	10	1.07 ± 0.04	1.62 ± 0.08	3.44 ± 0.04	2.03 ± 0.11
		50	2.18 ± 0.05	2.96 ± 0.15	8.27 ± 0.10	4.83 ± 0.07
		100	2.85 ± 0.07	3.97 ± 0.04	8.99 ± 0.20	5.77 ± 0.17
	100	10	1.43 ± 0.04	2.13 ± 0.05	4.33 ± 0.20	3.79 ± 0.09
		50	3.63 ± 0.04	5.14 ± 0.13	8.46 ± 0.18	5.76 ± 0.13
		100	4.55 ± 0.15	6.44 ± 0.29	9.76 ± 0.29	7.05 ± 0.09
bamboo	50	10	1.86 ± 0.06	1.52 ± 0.08	3.89 ± 0.09	2.53 ± 0.08
		50	2.93 ± 0.03	2.53 ± 0.05	6.23 ± 0.12	3.98 ± 0.09
		100	3.43 ± 0.09	3.00 ± 0.10	7.00 ± 0.11	4.93 ± 0.24
	100	10	2.03 ± 0.06	1.59 ± 0.08	4.09 ± 0.06	2.27 ± 0.07
		50	4.46 ± 0.12	3.86 ± 0.08	6.88 ± 0.22	5.97 ± 0.29
		100	5.29 ± 0.23	4.49 ± 0.19	7.48 ± 0.23	6.53 ± 0.13

[a]Mean ± standard of error (n = 3).

https://doi.org/10.1021/acsomega.3c02685
ACS Omega 2023, 8, 28467−28474

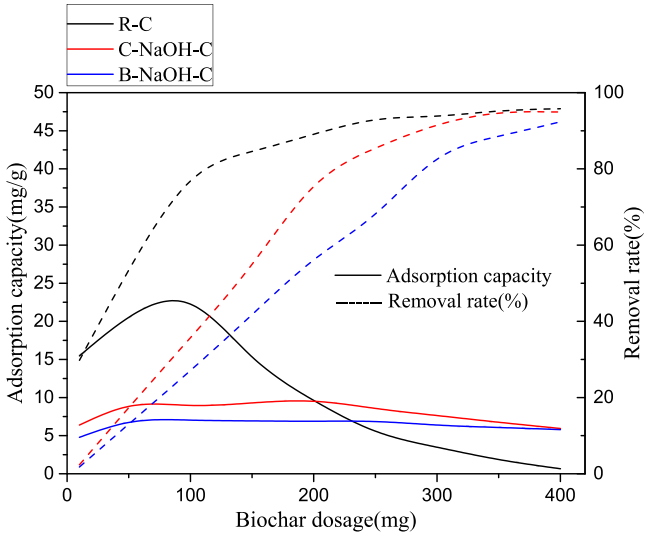

Figure 1. Effect of biochar dosage on adsorption of Mn^{2+} by R-C, C-NaOH-C, and B-NaOH-C.

From the adsorption capacity of manganese ions by three kinds of biochar, when the dosage of biochar exceeded 50 mg, the increase of adsorption capacity was not obvious. Considering the removal efficiency, the appropriate R-C, C-NaOH-C, and B-NaOH-C dosage is 50 mg when the concentration of Mn^{2+} in solution is 50 mg/L.

3.4. Effect of pH. In the process of adsorption, solution pH is the most important factor. It not only affects the surface properties of the adsorbent but also affects the ion exchange process. The effects of pH on the adsorption of Mn^{2+} by three biochar samples are displayed in Figure 2.

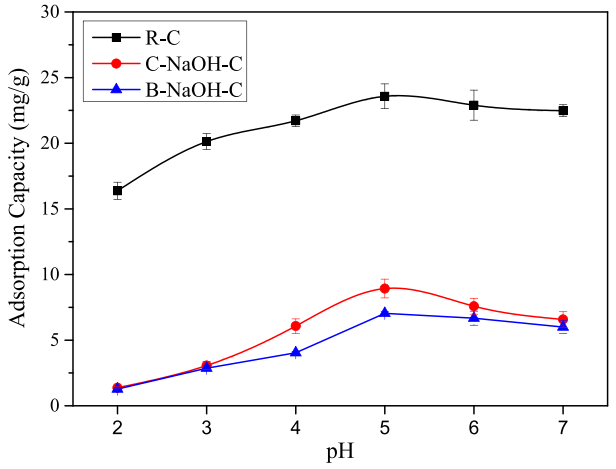

Figure 2. Effect of initial pH on adsorption of Mn^{2+} by R-C, C-NaOH, and B-NaOH-C.

From Figure 2, the adsorption capacity of manganese ions by R-C, C-NaOH-C, and B-NaOH-C increased and then decreased with the increase of pH. When the pH was 5, the adsorption capacities of manganese ions by R-C, C-NaOH-C, and B-NaOH-C were the maximum, 22.11, 8.93, and 7.04 mg/g, respectively. At pH from 1 to 5, the adsorption of manganese ions by the three biochar samples increased rapidly. It may be due to an increase in the pH, and the degree of ionization of the surface of the biochar increased, which exposes biochar to more and more surface-active sites. In addition, when the pH was low, a large amount of H^+ existed in the aqueous solution; H^+ had a higher migration conversion rate than metal ions and competed with metal ions for adsorption sites. Therefore, the competition gradually decreased as the pH increase, and the adsorption of manganese ions by biochar increased. The results of Chen et al.[14] also showed that as the pH increased, metal ions were more likely to replace protons on the surface of the adsorbent. When the pH was above 5, the adsorption capacity of manganese ions by R-C, C-NaOH-C, and B-NaOH-C decreased. It may be that when the pH was above a certain value, the negatively charged ions in the solution increased and the manganese ions might be surrounded by the anions in the solution, which were difficult to combine with the negatively charged adsorption sites of biochar. Therefore, the adsorption capacity of Mn^{2+} by biochar increased first and then decreased. When the pH of solution is above 7, the manganese ions easily transform to hydroxide precipitation.[30]

3.5. Effect of Temperature. In the process of adsorption, it is often associated with the variation of the energy, and the effect of temperature on the reaction rate is significant. The results of different temperatures (at 20, 25, 30, 35, and 40 °C) on the manganese ion adsorption by three biochar samples are shown in Figure 3.

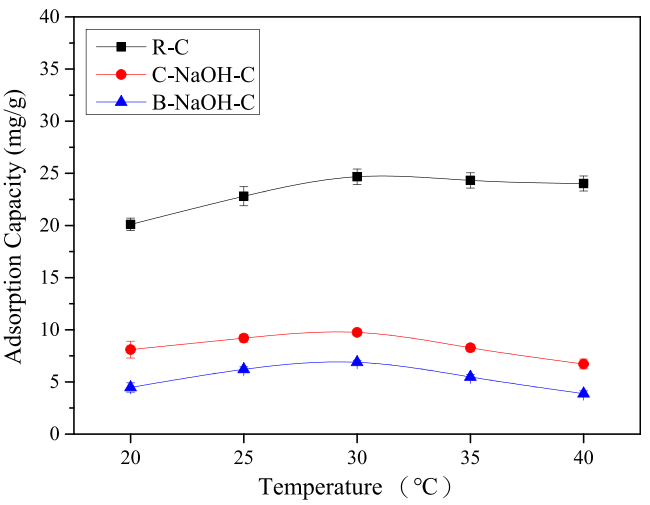

Figure 3. Effect of temperature on adsorption of Mn^{2+} by R-C, C-NaOH, and B-NaOH-C.

Figure 3 indicates that the adsorption capacity of manganese ions by three biochar samples increased first and then decreased with the increase of temperature. The adsorption capacities of obtained biochar are influenced by temperature. At 30 °C, the adsorption capacities of Mn^{2+} by R-C, C-NaOH, and B-NaOH-C were the maximum, and the maximum adsorption capacities were 24.68, 9.75, and 6.88 mg/g, respectively. In the process of adsorption, chemisorption is an endothermic reaction, the temperature rise is favorable for adsorption, physical adsorption is an exothermic reaction, and the temperature rise is unfavorable for adsorption. From the data of temperature on adsorption, it can be inferred that the adsorption processes of manganese ions by R-C, C-NaOH-C, and B-NaOH-C are accompanied by chemical adsorption and physical adsorption. The temperature of the environment plays an important role in the process of absorbing. Under the

https://doi.org/10.1021/acsomega.3c02685
ACS Omega 2023, 8, 28467−28474

combined action, 30 °C is the optimum for the adsorption by biochar.

3.6. Adsorption Kinetics. To explore the mechanism of Mn^{2+} removal, adsorption equilibrium experiments with R-C, C-NaOH-C, and B-NaOH-C were carried out. The isotherm curves by fitting the data with three adsorption models (quasi-first-order, quasi-second-order, and intraparticle diffusion models) are displayed in Figure 4; the corresponding parameters are calculated and summarized in Table 3.

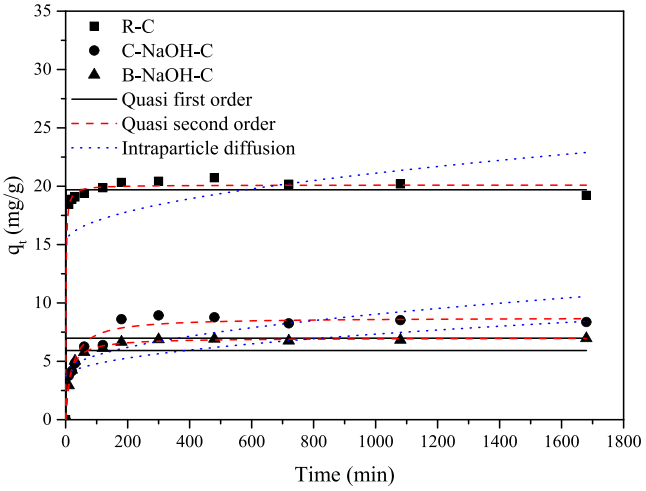

Figure 4. R-C, C-NaOH-C, and B-NaOH-C adsorption kinetic curves.

Figure 4 indicates that the initial adsorption rate of manganese ions by the three biochar samples is very rapid and achieved the adsorption equilibrium at about 180 min. At the stage of rapid adsorption, there are enough active binding sites on the surface of biochar.

The quasi-first-order reaction kinetic model, pseudo-second-order kinetic model, and intraparticle diffusion model are the most commonly used kinetic models to investigate the adsorption process of metal ions by adsorbents. In the quasi-first-order reaction kinetic equation, it is suggested that for the process of ions from the liquid phase to absorbents, the rate at which metal ions occupy the surface-active sites of the adsorbent is proportional to the number of adsorbed sites on the adsorbent that are not occupied. The equation of the quasi-first-order reaction kinetic model can be expressed as follows (eq 5):

$$q_t = q_e[1 - \exp(-K_1 t)] \quad (5)$$

q_e (mg/g) is the equilibrium adsorption capacity of metal ions, q_t (mg/g) is the capacity of metal ions adsorbed at any time, and K_1 (1/min) is the rate constant during the adsorption process.

The quasi-second-order kinetic model assumes that chemisorption is the main rate-adjusting step in the adsorption process; this involves the process of generating valence forces when electrons are exchanged and shared between the adsorbent and the adsorbate. The equation of the quasi-second-order kinetic model can be expressed as follows (eq 6):

$$q_t = \frac{q_e^2 K_2 t}{1 + q_e K_2 t} \quad (6)$$

q_e (mg/g) is the equilibrium adsorption capacity of metal ions, q_t (mg/g) is the capacity of metal ions adsorbed at any time, and K_2 (mg/(g·min)) is the rate constant during the adsorption process.

The intraparticle diffusion model can be used to investigate the diffusion of metal ions inside the adsorbent after they migrate from the liquid phase to the solid particle in the process of adsorption. The equation of the intraparticle diffusion model can be expressed as eq 7:

$$q_t = K_p t^{1/2} + c \quad (7)$$

q_t (mg/g) is the adsorption capacity of metal ions at any time, K_p (mg/(g·min$^{1/2}$)) is the rate constant of the internal diffusion model, and C (mg/g) is a constant related to the boundary.

Fitting the adsorption process of manganese ions by R-C, C-NaOH-C, and B-NaOH-C, three kinds of biochar with quasi-first-order, quasi-second-order, and intraparticle diffusion models, respectively, and the parameters obtained are shown in Table 3.

Table 3 indicates that the quasi-first-order kinetic model is more suitable for the adsorption of manganese ions by R-C, the correlation coefficient R^2 is 0.989, and the obtained equilibrium adsorption capacity q_e is closer to the actual q_e value. For adsorption of manganese ions by C-NaOH-C and B-NaOH-C, the quasi-second-order kinetic model is more suitable, the correlation coefficient R^2 is 0.953 and 0.997, respectively, and the equilibrium adsorption q_e is also closer to the actual q_e value. The correlation coefficient R^2 of quasi-first-order and quasi-second-order kinetics indicated that physical adsorption and chemisorption were simultaneously present in the adsorption of Mn^{2+} by three biochar samples. The results of fitting with the intraparticle diffusion model were the worst.

3.7. Adsorption Isotherms. The isotherm adsorption curves of manganese ions by three biochar samples are displayed in Figure 5.

From Figure 5, the adsorption capacity of manganese ions by three biochar samples increased with the increase of manganese ion concentration. The trend of the adsorption capacity increased rapidly and then stabilized.

The Langmuir model, Freundlich model, and Temkin model are the most commonly used isothermal adsorption models for describing the equilibrium constants of adsorption processes and investigating the relationship between the adsorbate and

Table 3. Quasi-First-Order, Quasi-Second-Order, and Intraparticle Diffusion Model Parameters

	quasi-first-order			quasi-second-order			intraparticle diffusion		
biocharcoal	q_e (mg/g)	K_1 (1/min)	R^2	q_e (mg/g)	K_2 (mg/(g·min))	R^2	K_p (mg/(g·min))	C (mg/g)	R^2
R-C	19.855	0.253	0.989	19.700	1.017	0.983	0.026	19.261	0.105
C-NaOH-C	8.260	0.032	0.911	8.754	0.006	0.953	0.121	4.956	0.531
B-NaOH-C	6.673	0.049	0.979	7.012	0.011	0.997	0.078	4.600	0.497

https://doi.org/10.1021/acsomega.3c02685
ACS Omega 2023, 8, 28467−28474

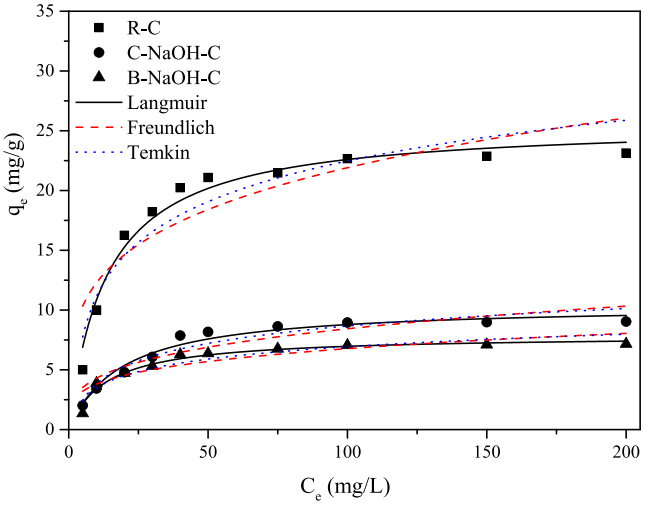

Figure 5. Adsorption isotherms.

adsorbent in the process of adsorption at a certain temperature.[22] The equation of the Langmuir model can be expressed as follows (eq 8):

$$q_e = \frac{q_m K_L C_e}{1 + K_L C_e} \tag{8}$$

q_e (mg/g) and q_m (mg/g) are the equilibrium adsorption capacity and maximum adsorption capacity of metal ions, respectively. C_e (mg/L) is the concentration of metal ions in solution during adsorption equilibrium, K_L is the equilibrium constant related to temperature and the properties of adsorbents and adsorbates. The greater the K_L value, the stronger the adsorption capacity of the adsorbent.

The Freundlich model is based on the empirical adsorption equilibrium model established by the adsorption of the adsorbate on multiphase surfaces. The equation of the Freundlich model can be expressed as follows (eq 9):

$$q_e = K_F C_e^{1/n} \tag{9}$$

q_e (mg/g) is the equilibrium adsorption capacity of metal ions, and K_F is the characteristic constant of the Freundlich equation, which can indicate the relative adsorption capacity of the adsorbent. $1/n$ can indicate the adsorption strength.

The Temkin model is used to evaluate the adsorption potential of the adsorbate on the adsorbent. The equation of the Temkin model can be expressed in the following (eq 10):

$$q_e = \frac{RT}{b} \ln K_T + \frac{RT}{b} \ln C_e \tag{10}$$

Q_e (mg/g) is the equilibrium adsorption capacity of metal ions, R (8.314 J/(mol·K)) is the constant, T (K) is the absolute temperature, b (J/mol) is the constant associated with the adsorption energy, and K_T (L/mg) is the equilibrium constant associated with the maximum binding energy.

The adsorption processes of manganese ions by R-C, C-NaOH-C, and B-NaOH-C were fitted with the Langmuir isotherm adsorption model, Freundlich isotherm adsorption model, and Temkin isotherm adsorption model, and the parameters obtained are shown in Table 4.

The correlation coefficients R^2 of the Langmuir isotherm adsorption model, Freundlich isotherm adsorption model, and Temkin isotherm adsorption model are 0.970, 0.964, and 0.958, respectively. It indicated that the Langmuir isotherm adsorption model was best suitable for the adsorption of manganese ions by R-C, C-NaOH-C, and B-NaOH-C. The maximum adsorption capacities of R-C, C-NaOH-C, and B-NaOH-C for manganese ions are 25.67, 10.45, and 7.89 mg/g, respectively. The K_F of the Freundlich equation reveals the relative adsorption capacity of the adsorbent, and the relative adsorption capacity of the three biochar samples can be seen from the table: R-C > C-NaOH-C > B-NaOH-C.

The parameter K_L in the Langmuir equation and the parameter n of the Freundlich equation can both indicate the strength of the adsorption. When n is less than 1, it indicates that the adsorption is difficult to react, and when n is more than 2, the adsorption by adsorbents is easy. From Table 3, the parameters n of the Freundlich equation for the adsorption of manganese ions by R-C, C-NaOH-C, and B-NaOH-C are more than 2, indicating that the adsorption of manganese ions by the three kinds of biochar is easy to carry out. The order of parameter K_L values in the Langmuir equation for the adsorption of manganese ions was B-NaOH-C > R-C > C-NaOH-C, indicating that the adsorption strength to manganese ions is B-NaOH-C > R-C > C-NaOH-C.

4. CONCLUSIONS

In conclusion, among the three modification methods, biochar modified with NaOH is the optimum for the adsorption of Mn^{2+}. However, the same method of modification has different effects on different biomass materials. For rice straw, R-C without modification has the maximum capacity. For coconut shell and fresh bamboo, biochar samples modified by NaOH are the optimum. There are significant differences among the adsorption capacity of these biochar adsorbents from different biomass feedstocks. The physical and surface chemical properties of biochar or biomass feedstock should be carefully considered in the selection of pretreatment methods. In the case of a manganese ion concentration of 50 mg/L in an aqueous solution, the optimum dosage for adsorption of manganese ions by three biochar samples is 50 mg; pH and temperature play an important role in the process of adsorption. The optimum pH of solution for the adsorption of manganese is 5, and the optimum temperature is 30 °C. The adsorption processes of Mn^{2+} by these biochar samples are fitted better with the Langmuir isothermal adsorption model. The kinetic model indicated that physical adsorption and

Table 4. Isothermal Adsorption Model Parameters of Langmuir, Freundlich, and Temkin

	Langmuir			Freundlich			Temkin		
biocharcoal	q_m (m/g)	K_L	R^2	K_F	n	R^2	B	K_T	R^2
R-C	25.674	0.073	0.970	6.900	3.986	0.772	503.921	0.967	0.885
C-NaOH-C	10.453	0.053	0.964	2.204	3.431	0.813	1179.616	0.620	0.913
B-NaOH-C	7.888	0.076	0.958	2.151	4.015	0.780	1653.699	0.976	0.887

https://doi.org/10.1021/acsomega.3c02685
ACS Omega 2023, 8, 28467−28474

chemisorption are simultaneously present in the adsorption process of the three biochar samples to manganese ions. Overall, the results obtained from this study suggest that the key of using biochar as adsorbents is to find the appropriate biomass feedstock.

AUTHOR INFORMATION

Corresponding Author

Guoliang Chen − *School of Resource & Environment and Safety Engineering and Hunan Province Key Laboratory of Coal Resources Clean-Utilization and Mine Environment Protection, Hunan University of Science and Technology, Xiangtan 411201, China;* orcid.org/0009-0004-5685-1522; Email: glchen@hnust.edu.cn

Authors

Khamphouvanh Viengvilay − *School of Resource & Environment and Safety Engineering, Hunan University of Science and Technology, Xiangtan 411201, China*

Weijian Yu − *School of Resource & Environment and Safety Engineering and Hunan Province Key Laboratory of Coal Resources Clean-Utilization and Mine Environment Protection, Hunan University of Science and Technology, Xiangtan 411201, China*

Teng Mao − *School of Resource & Environment and Safety Engineering, Hunan University of Science and Technology, Xiangtan 411201, China*

Zhihui Qu − *School of Resource & Environment and Safety Engineering, Hunan University of Science and Technology, Xiangtan 411201, China*

Bixin Liang − *School of Resource & Environment and Safety Engineering, Hunan University of Science and Technology, Xiangtan 411201, China*

Zhang Chen − *School of Resource & Environment and Safety Engineering and Hunan Province Key Laboratory of Coal Resources Clean-Utilization and Mine Environment Protection, Hunan University of Science and Technology, Xiangtan 411201, China*

Zhixian Li − *School of Resource & Environment and Safety Engineering and Hunan Province Key Laboratory of Coal Resources Clean-Utilization and Mine Environment Protection, Hunan University of Science and Technology, Xiangtan 411201, China;* orcid.org/0000-0002-5793-0052

Complete contact information is available at: https://pubs.acs.org/10.1021/acsomega.3c02685

Notes

The authors declare no competing financial interest.

ACKNOWLEDGMENTS

This work was supported by the Natural Science Foundation of Hunan Province China (no. 2023JJ30230), the Scientific Research Fund of Hunan Provincial Education Department (no. 21B0451), the Teaching Research and Reform Project of Hunan Province (HNJG-2022−0174), the Open Foundation of Hunan Province Key Laboratory of Coal Resources Clean-Utilization and Mine Environment Protection (no. E22301), and the National Natural Science Foundation of China (no. 41501343).

REFERENCES

(1) Jiang, F.; Ren, B.; Hursthouse, A.; Zhou, Y. Trace metal pollution in topsoil surrounding the Xiangtan manganese mine area (South-Central China), source identification, spatial distribution and assessment of potential ecological risks. *Int. J. Environ. Res. Public Health* **2018**, *15*, 2412.

(2) Li, Y.; Xu, Z.; Ma, H.; Hursthouse, A. S. Removal of manganese(II) from acid mine wastewater, a review of the challenges and opportunities with special emphasis on Mn-oxidizing bacteria and microalgae. *Water* **2019**, *11*, 2493.

(3) Luo, X.; Ren, B.; Hursthouse, A. S.; Thacker, J. R. M.; Wang, Z. Soil from an abandoned manganese mining area (Hunan, China), significance of health risk from potentially toxic element pollution and its spatial context. *Int. J. Environ. Res. Public Health* **2020**, *17*, 6554.

(4) Xie, Q.; Ren, B.; Hursthouse, A.; Shi, X. Effects of mining activities on the distribution, controlling factors, and sources of metals in soils from the Xikuangshan south mine, Hunan Province. *Integr. Environ. Assess. Manage.* **2022**, *18*, 748−756.

(5) Chen, Z.; Liu, T.; Tang, J.; Zheng, Z.; Wang, H.; Shao, Q.; Chen, G.; Li, Z.; Chen, Y.; Zhu, J.; Feng, T. Characteristics and mechanisms of cadmium adsorption from aqueous solution using lotus seedpod-derived biochar at two pyrolytic temperatures. *Environ. Sci. Pollut. Res.* **2018**, *25*, 11854−11866.

(6) Liu, L.; Liu, J.; Zhao, L.; Yang, Z.; Lv, C.; Xue, J.; Tang, A. Synthesis and characterization of magnetic Fe_3O_4@$CaSiO_3$ composites and evaluation of their adsorption characteristics for heavy metal ions. *Environ. Sci. Pollut. Res.* **2019**, *26*, 8721−8736.

(7) Zhang, J.; Deng, R.-J.; Ren, B.-Z.; Hou, B.; Hursthouse, A. Preparation of a novel Fe_3O_4/HCO composite adsorbent and the mechanism for the removal of antimony (III) from aqueous solution. *Sci. Rep.* **2019**, *9*, 13021.

(8) Luo, X.; Ren, B.; Hursthouse, A. S.; Jiang, F.; Deng, R.-j. Potentially toxic elements (PTEs) in crops, soil, and water near Xiangtan manganese mine, China, potential risk to health in the foodchain. *Environ. Geochem. Health* **2020**, *42*, 1965−1976.

(9) Chen, C.; Peng, Z.; Gu, J. Y.; Peng, Y.; Wu, L. Exploring environmentally friendly biopolymer material effect on soil tensile and compressive behavior. *Int. J. Environ. Res. Public Health* **2020**, *17*, 9032.

(10) Liu, T.; Chen, Z.; Li, Z.; Fu, H.; Chen, G.; Feng, T.; Chen, Z. Preparation of magnetic hydrochar derived from iron-rich *Phytolacca acinosa* Roxb. for Cd removal. *Sci. Total Environ.* **2021**, *769*, No. 145159.

(11) Deng, R.; Shao, R.; Ren, B.; Hou, B.; Tang, Z.; Hursthouse, A. Adsorption of Antimony(III) onto Fe(III)-Treated Humus Sludge Adsorbent, Behavior and Mechanism Insights. *Pol. J. Environ. Stud.* **2019**, *28*, 10.

(12) Zhang, Y.; Zhao, C.; Chen, G.; Zhou, J.; Chen, Z.; Li, Z.; Zhu, J.; Feng, T.; Chen, Y. Response of soil microbial communities to additions of straw biochar, iron oxide, and iron oxide−modified straw biochar in an arsenic-contaminated soil. *Environ. Sci. Pollut. Res.* **2020**, *27*, 23761−23768.

(13) Zhu, G.; Lin, J.; Yuan, Q.; Wang, X.; Zhao, Z.; Hursthouse, A. S.; Wang, Z.; Li, Q. A biochar supported magnetic metal organic framework for the removal of trivalent antimony. *Chemosphere* **2021**, *282*, No. 131068.

(14) Chen, G.; Ma, Y.; Xu, W.; Chen, Z.; Li, Z.; Zhou, J.; Yu, W. Remediation of cadmium-contaminated soil by micro-nano nitrogen-doped biochar and its mechanisms. *Environ. Sci. Pollut. Res.* **2023**, *30*, 48078−48087.

(15) Du, J.; Wang, C.; Zhao, Z.; Chen, R.; Zhang, P.; Cui, F. Effect of vacuum ultraviolet/ozone pretreatment on alleviation of ultrafiltration membrane fouling caused by algal extracellular and intracellular organic matter. *Chemosphere* **2022**, *305*, No. 135455.

(16) Jiang, F.; Ren, B.; Hursthouse, A.; Deng, R.; Wang, Z. Distribution, source identification, and ecological-health risks of potentially toxic elements (PTEs) in soil of thallium mine area (southwestern Guizhou, China). *Environ. Sci. Pollut. Res.* **2019**, *26*, 16556−16567.

https://doi.org/10.1021/acsomega.3c02685
ACS Omega 2023, 8, 28467−28474

(17) Li, Y.; Yang, X.; Geng, B. Preparation of immobilized sulfate-reducing bacteria-microalgae beads for effective bioremediation of copper-containing wastewater. *Water, Air, Soil Pollut.* **2018**, *229*, 54.
(18) Meng, D.; Li, J.; Liu, T.; Liu, Y.; Yan, M.; Hu, J.; Li, X.; Liu, X.; Liang, Y.; Liu, H.; Yin, H. Effects of redox potential on soil cadmium solubility, Insight into microbial community. *J. Environ. Sci.* **2019**, *75*, 9.
(19) Chen, G.; Ran, Y.; Ma, Y.; Chen, Z.; Li, Z.; Chen, Y. Influence of *Rahnella aquatilis* on arsenic accumulation by *Vallisneria natans* (Lour.) Hara for the phytoremediation of arsenic-contaminated water. *Environ. Sci. Pollut. Res.* **2021**, *28*, 44354−44360.
(20) Chen, Z.; Li, Z.; Chen, G.; Zhu, J.; Liu, Q.; Feng, T. In situ formation of AgNPs on *S. cerevisiae* surface as bionanocomposites for bacteria killing and heavy metal removal. *Int. J. Environ. Sci. Technol.* **2017**, *14*, 1635−1642.
(21) Zhang, Y.; Huang, F. Indicative significance of the magnetic susceptibility of substrate sludge to heavy metal pollution of urban lakes. *Scienceasia* **2021**, *47*, 9.
(22) Chen, Y.; Cao, J.; Zhao, J.; Wu, J.; Zou, X.; Fu, S.; Zhang, W. Labile C dynamics reflect soil organic carbon sequestration capacity, Understory plants drive topsoil C process in subtropical forests. *Ecosphere* **2019**, *10*, No. e2784.
(23) Chen, G.; Feng, T.; Li, Z.; Chen, Z.; Chen, Y.; Wang, H.; Xiang, Y. Influence of sulfur on the arsenic phytoremediation using *Vallisneria natans* (Lour.) Hara. *Bull. Environ. Contam. Toxicol.* **2017**, *99*, 411−414.
(24) Zhu, J.; Wallis, I.; Guan, H.; Ross, K.; Whiley, H.; Fallowfield, H. Juncus sarophorus, a native Australian species, tolerates and accumulates PFOS, PFOA and PFHxS in a glasshouse experiment. *Sci. Total Environ.* **2022**, *826*, No. 154184.
(25) Yu, H.; Xiang, Y.; Zou, D. The effect of *Eulaliopsis binata* on the physi-chemical properties, microbial biomass, and enzymatic activities in Cd-Pb polluted soil. *Environ. Sci. Pollut. Res.* **2016**, *23*, 19212−19218.
(26) Yu, S.; Chen, Y.; Zhao, J.; Fu, S.; Li, Z.; Xia, H.; Zhou, L. Temperature sensitivity of total soil respiration and its heterotrophic and autotrophic components in six vegetation types of subtropical China. *Sci. Total Environ.* **2017**, *607-608*, 160−167.
(27) Li, X.; Meng, D.; Li, J.; Yin, H.; Liu, H.; Liu, X.; Cheng, C.; Xiao, Y.; Liu, Z.; Yan, M. Response of soil microbial communities and microbial interactions to long-term heavy metal contamination. *Environ. Pollut.* **2017**, *231*, 908−917.
(28) Chen, Y.; Zhang, Y.; Cao, J.; Fu, S.; Hu, S.; Wu, J.; Zhao, J.; Liu, Z. Stand age and species traits alter the effects of understory removal on litter decomposition and nutrient dynamics in subtropical Eucalyptus plantations. *Global Ecol. Conser.* **2019**, *20*, No. e00693.
(29) Zhou, Y.; Ren, B.; Hursthouse, A.; Zhou, S. Antimony ore tailings, heavy metals, chemical speciation, and leaching characteristics. *Pol. J. Environ. Stud.* **2019**, *28*, 485−495.
(30) Deng, R.-J.; Jin, C.-S.; Ren, B.-Z.; Hou, B.-L.; Hursthouse, A. S. The potential for the treatment of antimony-containing wastewater by iron-based adsorbents. *Water* **2017**, *9*, 794.

https://doi.org/10.1021/acsomega.3c02685
ACS Omega 2023, 8, 28467−28474